PSFC/JA-15-58

# The physics mechanisms of the weakly coherent mode in the Alcator C-Mod Tokamak

Liu, Z.X.,[*] Xu, X.Q.,[**] Gao, X.,[*] Hubbard, A.E.,
Hughes, J.W., Walk, J.R., Theiler, C., Xia, T.Y.,[*] Baek, S.G.,
Golfinopoulos, T., Whyte, D., Zhang, T.,[*] Li, J.G.[*]

* Institute of Plasma Physics, Chinese Academy of Sciences
** Lawrence Livermore National Laboratory

December, 2015

**Plasma Science and Fusion Center**
**Massachusetts Institute of Technology**
**Cambridge MA 02139 USA**

*Submitted to Nuclear Fusion*

This work was supported by the National Magnetic Confinement Fusion Program of China (Grant Nos. 2014GB106001, 2014GB106003), the National Natural Science Foundation of China (Grant Nos. 11021565, 11275234, 11405213, 11405215, 11405217, and 11422546) and the U.S. Department of Energy (Grant Nos. DE-AC52-07NA27344, LLNL-PRES-669975, and DE-FC02-99ER54512). 

# The physics mechanisms of the weakly coherent mode in the Alcator C-Mod Tokamak

Z. X. Liu*,[1,2] X. Q. Xu,[2] X. Gao,[1] A. E. Hubbard,[3] J. W. Hughes,[3] J. R. Walk,[3] C. Theiler,[3] T. Y. Xia,[1,2] S. G. Baek,[3] T. Golfinopoulos,[3] D. Whyte,[3] T. Zhang,[1] and J. G. Li[1]

[1]*Institute of Plasma Physics, Chinese Academy of Sciences, Hefei 230031, China*
[2]*Lawrence Livermore National Laboratory, Livermore, California 94550, USA*
[3]*MIT Plasma Science and Fusion Center, Cambridge MA, USA*

The weakly coherent mode (WCM) in I-mode has been studied by a six-field two-fluid model based on the Braginskii equations under the BOUT++ framework for the first time. The calculations indicate that a tokamak pedestal exhibiting a WCM is linearly unstable to drift Alfven wave (DAW) instabilities and the resistive ballooning mode. The nonlinear simulation shows promising agreement with the experimental measurements of the WCM. The power spectral density of the dominant toroidal number mode $n$=20 at the location of the reflectometry agrees with the experimental data. That the simulated mode propagates in electron diamagnetic direction is consistent with the results from the magnetic probes in the laboratory frame, a large ratio of particle to heat diffusivity is consistent with the distinctive experimental feature of I-mode, and the value of $\chi_e$ from the simulation is almost the same as $\chi_{eff}$ from the experiment. The prediction of the WCM shows that free energy is mainly provided by the electron pressure gradient, which gives a well guidance for pursuing future I-mode studies.

I-mode [1, 2], explored on the Alcator C-Mod tokamak [3] as well as ASDEX Upgrade[4] and DIII-D[5], is a promising alternative regime for ITER and reactor-scale operation, characterized by its apparent decoupling of energy and particle transport, which results in good energy confinement without impurity accumulation. The regime is naturally stable to Edge Localized Modes. I-mode is accompanied by a reduction in edge turbulence in the mid-frequency range of $50-200$kHz and usually exhibits a higher-frequency (about $200-400$kHZ) fluctuation, dubbed the "weakly-coherent mode" (WCM) [1, 6–8]. The WCM is well characterized experimentally on C-Mod, with density, temperature, and magnetic fluctuations visible on multiple diagnostics [7–9]. The density fluctuation is typically stronger by a factor of 5-10 [8]. Recent MHD calculations using the ELITE code [10] indicate that I-mode pedestals are strongly stable to edge peeling-ballooning instabilities and ideal ballooning mode calculations suggest stability to the kinetic ballooning mode (KBM). Cross-bispectral measurements of the spectral transfer of density fluctuations showed that the geodesic-acoustic mode (GAM) is responsible for the broadened frequency structure of the WCM [8]. But the underlying physics basis of the WCM has been poorly understood.

The three-field model under the BOUT++ framework [11, 12] has successfully simulated the nonlinear crash phase of ELMs [13, 14], which is mainly driven by the Peeling-Ballooning mode. In this paper, the electromagnetic six-field two-fluid model, including more physics such as ion acoustic waves, thermal conductivities, Hall effect, compressibility, and electron-ion friction, has been used to simulate the WCM and elucidate the nature and underlying physics mechanisms. The equations used here are given explicitly in Ref. [14].

In this letter, the equilibrium of C-Mod I-mode discharge No. 1120907032 is used for the simulations. The discharge parameters are $I_P = 1.1$MA, $B_T = 5.8$T, average additional heating power $P_{ICRF} = 5$MW. The geometry of this discharge is lower single-null with the $B\times\nabla B$ drift directed away from the active X-point. The time evolution of the mode frequency spectrum is shown in Fig. 1 (a). The WCM typically appears with a frequency centered on 350kHz following the transition from the "low confinement" (L-mode) to the I-mode at 0.75s. The toroidal mode number of the WCM is from $n$=15 to 25 propagating in the electron diamagnetic drift direction in the laboratory frame, as diagnosed by magnetic probes, and the effective average of $\chi_i$ (iron thermal diffusivity) and $\chi_e$ (electron thermal diffusivity) is around 0.2 $m^2/s$ measured from a power balance across the pedestal region ($r/a = 0.95-1$) as shown in Fig. 1 (b) and (c). We use quasi-neutrality ($n_e = n_i$) and flat profiles in the SOL region as "model assumptions", so the profiles in the simulation (solid red curves in Fig. 2) are a little different from the experimental data (dashed blue curve in Fig. 2). Applying new BOUT++ capability including impurity species and the real profile in the SOL region will be future work.

Linear simulations with ideal MHD terms (black dashed curve with crosses in Fig. 3) show zero growth rates indicating that there is no Peeling-Ballooning mode, which is consistent with the absence of ELMs in the I-mode phase. When all terms in the six-field model are considered, a strong instability (solid red curve with square in Fig. 3) exists at $n \geq 20$. From testing of the terms in the six-field model separately, we found

*Author to whom correspondence should be addressed; electronic mail: zxliu316@ipp.ac.cn

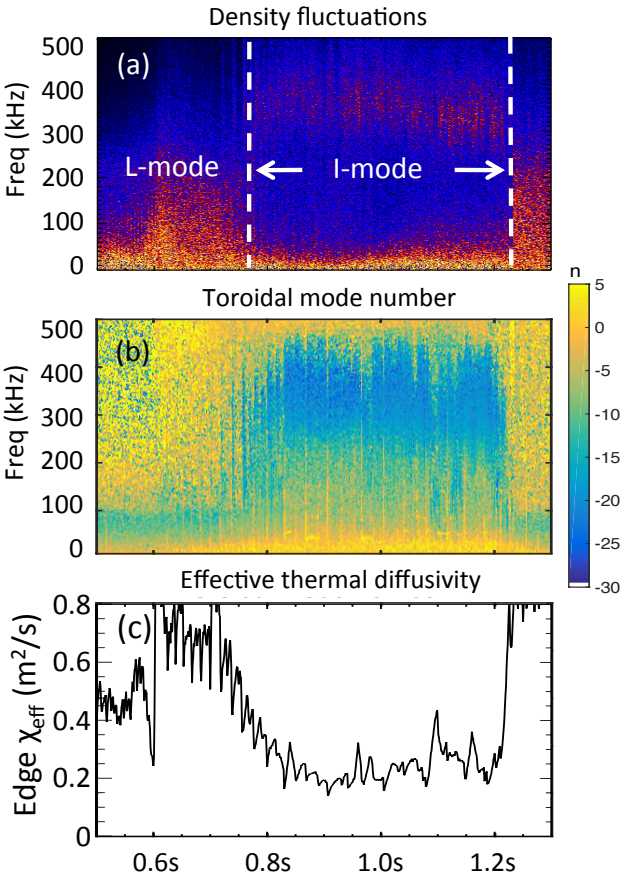


FIG. 1: (a) Spectrum of the density fluctuation mode diagnosed from reflectometry at $\psi = 0.988$; (b) Toroidal numbers of the modes calculated by data from magnetic probes; (c) Effective thermal diffusivity $\chi_{eff}$ from a power balance across the pedestal region ( $r/a$ from 0.95 to 1) and assuming power is split between ion and electron channels.

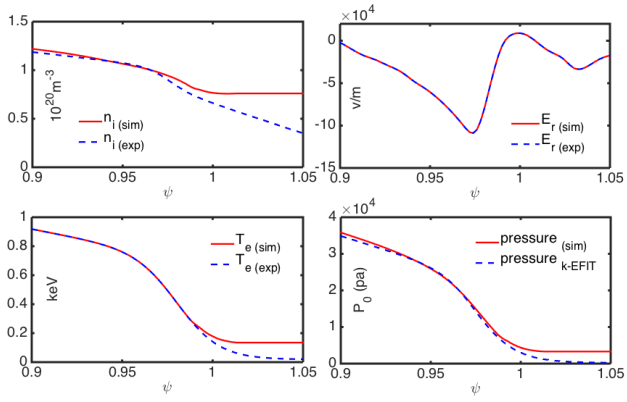


FIG. 2: Profiles in the simulation. Solid red curves are the profiles in the simulation, and dashed blue curves are the profiles from the experiment.

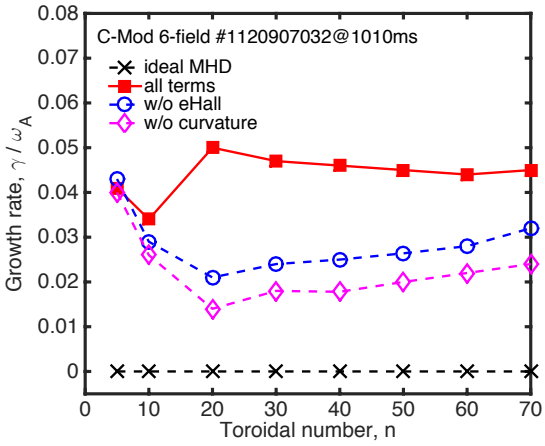


FIG. 3: Growth rate vs toroidal mode number in linear BOUT++ simulations. The black dashed curve with crosses is the case with ideal MHD; red solid curve with squares is the case with all terms in the six-field model; blue dashed curve with circles is the case without the eHall term; and the pink dashed curve with diamonds is the case without the curvature term.

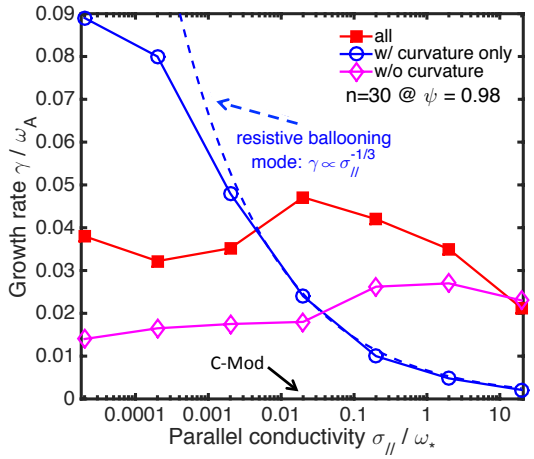


FIG. 4: Growth rate vs parallel conductivity. Red solid curve with squres is the case with all terms in the six-field model; blue solid curve with circles is the case with the curvature term only; and pink dashed curve with diamonds is the case without the curvature term.

that the eHall (electron Hall effects) term and the curvature term are the most important contributions. Parallel conductivity normalized by the diamagnetic frequency $\omega_* = kT_{e0}/L_N$[15] has been scanned and used to identify the mode. The scan with all terms shows a complex behavior as shown in Fig. 4, but the scan with curvature only shows good agreement with the theory of the resistive ballooning mode[16] at $\sigma_\parallel/\omega_* > 0.002$. The scan without curvature has a peak at $\sigma_\parallel/\omega_* = 2$, which is similar to the trend of the theory of the collisional drift wave[17] (it might be modified by other

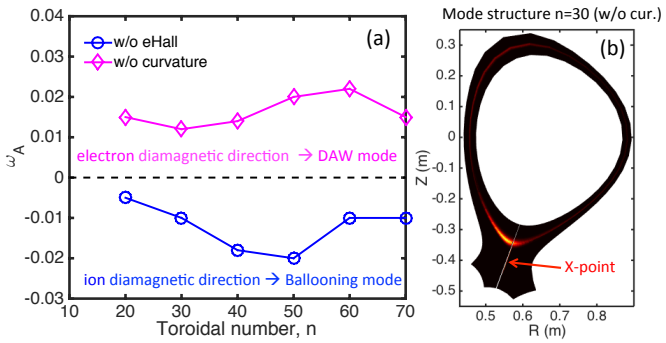


FIG. 5: (a) Frequency of the mode without eHall and without curvature; (b) Mode amplitude structure at $n$=30 without curvature in the linear simulation.

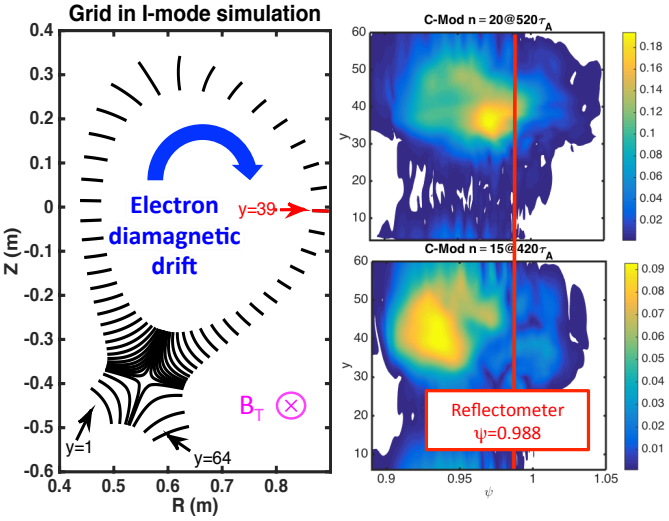


FIG. 6: Distribution of density fluctuations from the contribution of $n$=15 and $n$=20. The black curves in the left figure shows the grid in the simulation, which is the y axis on other figures. The left figure also shows the direction of the electron diamagnetic drift and $B_T$. The position of the outer mid-plane is $y$=39.

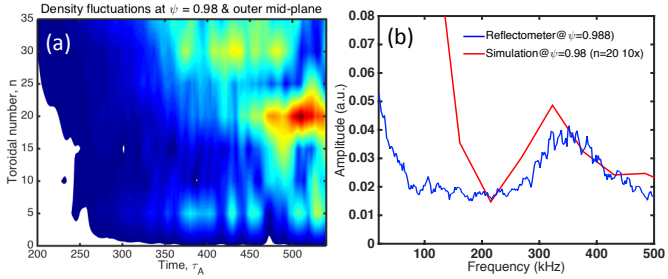


FIG. 7: (a) Time evolution of simulated density fluctuation amplitude of the modes from $n$=5 to 35. (b) The red curve is the frequency spectrum of density fluctuation from the simulated mode $n$=20 at $\psi = 0.98$ (outer mid-plane), and the blue curve is the frequency spectrum of the density fluctuation diagnosed by reflectometry at $\psi = 0.988$ (outer mid-plane).

terms). The propagation direction of the frequency in the plasma frames ($E_r = 0$) is another way to identify the mode. Figure 5 (a) shows that mode without the curvature term propagates in the electron diamagnetic drift direction, which is in agreement with the drift Alfven wave (DAW) instability, while mode without the eHall term propagates in the ion diamagnetic direction, which is in agreement with ballooning mode. In addition, the eigenmode at $n = 30$ without curvature mainly peaks at the X-point and has a smaller component at the top of the machine as shown in Fig. 5 (b), which is consistent with the eigenmode structure of the DAW instability described in the Gyrokinetic Toroidal Code (GTC) test [18]. Taken together, these tests indicate that the I-mode edge is linearly unstable to both the DAW instability and the resistive ballooning mode.

In order to compare the simulation results with the diagnostic measurements from the experimental measurements, nonlinear simulations have been performed. Figure 6 shows that the radial and poloidal locations of the peaks of the density fluctuations vary with mode number: $n$=20 peaks around $\psi = 0.98$ while $n$=15 peaks around $\psi = 0.94$ the outer midplane, in contrast to linear simulations. The different poloidal locations of the perturbation between the linear and nonlinear simulations should arise because of the flow of the nonlinear poloidal fluxes from top and bottom toward the mid-plane, leading to a nonlinear perturbation near the mid-plane. The time evolution of the density fluctuation of the modes from $n$ = 5 to 35 at $\psi = 0.98$ (outer mid-plane) is shown in Fig. 7 (a), a contour plot of density fluctuation amplitude vs toroidal mode number $n$ and time at the peak gradient position $\psi = 0.98$ at outer mid-plane. It is clearly shown that the most unstable mode number at the edge shifts from $n$=30 during the linear phase to $n$=20 in the nonlinear phase because of an inverse cascade[19, 20]. Figure 7 (b) shows the frequency spectrum of the $n = 20$ mode (red curve) at $\psi = 0.98$ and the frequency spectrum of the reflectometry[7, 21] measurements (blue curve) at $\psi = 0.988$ (outer mid-plane). The two curves almost peak at the same frequency indicating rough agreement between the simulation and the experiment. The direction of the predicted fluctuation is clockwise, aligned with the electron diamagnetic drift velocity, and the normalized density fluctuation from the simulation is about 10 times larger than the electron temperature fluctuation (details have been presented in Ref. [22]). These features also agree with the experimental results.

Transport has been calculated from the nonlinear simulation. The solid curves in Fig. 8 are the particle diffusivities $D_e$ and $D_i$, and the dashed curves are the thermal diffusivities $\chi_e$ and $\chi_i$. The particle diffusivity is larger than the thermal, which is consistent with the key feature of I- mode. Predicted $\chi_e$ and $\chi_i$ roughly agree with

the experimental $\chi_{eff}$ over $\psi = 0.95$ to 1(dashed black rectangle). Figure 9 shows that the fluctuation of the electron temperature is almost in phase with the electric potential from $425\tau_A$ to $525\tau_A$, which means the electric potential drives the electron temperature directly.

The DAW is sensitive to the gradient of $T_e$ [23], but less sensitive to $T_i$. To clearly illustrate the correspondence, we have performed linear BOUT++ simulations for a scan of $T_e$ and $T_i$ with the toroidal mode number $n$=30, resistivity held fixed. The dashed black curve in Fig. 10 shows that the growth rate changes slightly with increasing $T_e$ profile scale if we use the calculated $T_i$ profile ($T_i = P/n_e - T_e$) to keep the same pressure profile. The solid curves show that the growth rate has increased when the electron and ion increase separately, without enforcing self-consistence (no calculated $T_i$ or $T_e$ to offset the change). These scans enhance the total pressure, but the larger/faster increase of the growth rate in the $T_e$ scan still indicates that the free energy for the mode is mainly from the electron pressure gradient, and increasing $T_e$ at the edge should increase the WCM intensity. This result suggests that, in devices which have auxiliary heating predominately on ions and which have weak ion-electron coupling, additional electron heating may facilitate I-mode access. Note that C-Mod is primarily electron-heated and has strong ion-electron coupling, and routinely accesses I-mode.

In conclusion, BOUT++ simulations have been performed to elucidate the nature and underlying physics mechanisms of the WCM, which causes particle transport in I-mode pedestals of Alcator C-Mod. Key simulation results are that from the linear simulation, there is no ideal peeling-ballooning mode instability for the I-mode studied in agreement with[10]; a strong instability exists at $n \geq 20$; I-mode edge with WCM is unstable to both the DAW instability and the resistive ballooning mode; the free energy for the WCM is mainly provided by the electron pressure gradient; from the nonlinear simulation, the mode propagates in the electron diamagnetic direction; the predicted frequency of the $n = 20$ mode agrees with the measured WCM peaks around 350kHz; the predicted $\chi_e$ agrees with the $\chi_{eff}$ from the experiment; and the predicted particle transport is larger than the predicted heat transport. The simulation results are subjected to the following assumptions and further improvement will be made in future work. The net equilibrium zonal flow is set to be zero, so the interaction of the WCM with GAMs is not included. A fixed radial electric potential ($E_r$) profile has been used that makes the system in the nonlinear simulation not self-consistent.

The authors wish to acknowledge Drs. Ben Dudson and M. V. Umansky for their contribution to the BOUT++ framework, Mr. E. Davis for useful physics discussions. This work was supported by the National Magnetic Confinement Fusion Program of China (Grant Nos. 2014GB106001, 2014GB106003), and the National Natural Science Foundation of China (Grant Nos. 11021565, 11275234, 11405213, 11405215, 11405217, and 11422546), and was performed under the auspices of the U.S. Department of Energy by Lawrence Livermore National Laboratory under Contract DE-AC52-07NA27344, This material is based upon work supported by the U.S. Department of Energy, Office of Science, Office of Fusion Energy Sciences. LLNL-PRES-669975, and US DoE Cooperative Agreement for Alcator C-Mod. DE-FC02-99ER54512.

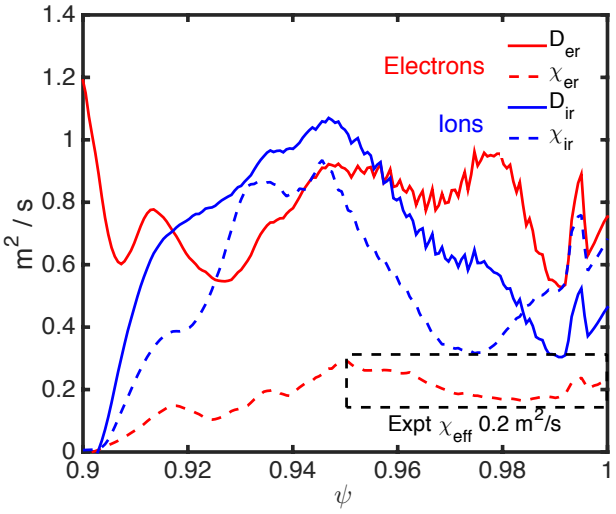


FIG. 8: Predicted particle and thermal diffusivities near the edge. The experimental range of values is indicated by the dashed black rectangle.

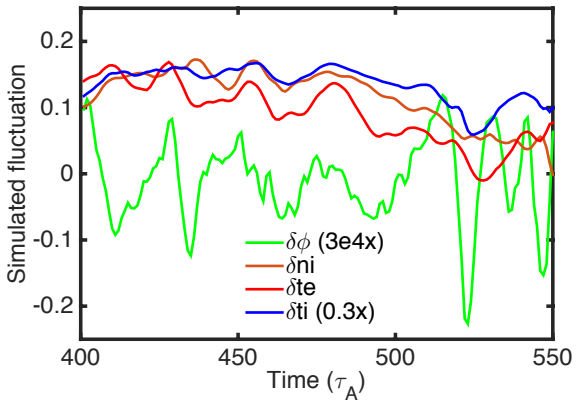


FIG. 9: Simulated fluctuations of electric potential, density, electron temperature, and ion temperatue.

[1] D. Whyte, A. Hubbard, J. Hughes, B. Lipschultz, J. Rice, E. Marmar, M. Greenwald, I. Cziegler, A. Dominguez, T. Golfinopoulos, N. Howard, L. Lin, R. McDermott, M.

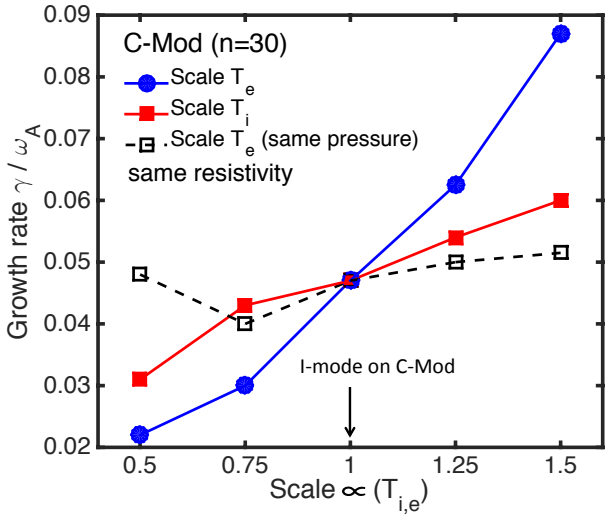


FIG. 10: Growth rate vs $T_i$ and $T_e$ with same resistivity.


Porkolab, M. Reinke, J. Terry, N. Tsujii, S. Wolfe, S. Wukitch, Y. Lin, and the Alcator C-Mod Team, Nuclear Fusion 50, 105005 (2010).

[2] R. M. McDermott, Edge radial electric field studies via charge exchange recombination spec- troscopy on the Alcator C-Mod tokamak, Ph.D. thesis, Massachusetts Institute of Technology (2009).

[3] E. S. Marmar, Alcator C-Mod Group, Fusion Science and Technology, 51, 261 (2007).

[4] P. Manz, P. Lauber, V. E. Nikolaeva, T. Happel, F. Ryter, G. Birkenmeier, A. Bogomolov, G. D. Conway, M. E. Manso, M. Maraschek, D. Prisiazhniuk, E. Viezzer and the ASDEX Upgrade Team, Nucl. Fusion, 55, 083004 (2015)

[5] A. Marinoni, J. C. Rost, M. Porkolab, A. E. Hubbard, T. H. Osborne, A. E. White, D. G. Whyte, T. L. Rhodes, E. M. Davis, D. R. Ernst, K. H. Burrell and the DIII-D Team, Nucl. Fusion, 55, 093019 (2015) .

[6] A. E. Hubbard, D. G. Whyte, R. M. Churchill, I. Cziegler, A. Dominguez, T. Golfinopoulos, J. W. Hughes, J. E. Rice, I. Bespamyatnov, M. J. Greenwald, N. Howard, B. Lipschultz, E. S. Marmar, M. L. Reinke, W. L. Rowan, J. L. Terry and Alcator C-Mod Group, Physics of Plasmas, 18, 056115 (2011).

[7] A. Dominguez, Study of Density Fluctuations and Particle Transport at the Edge of I-Mode Plasmas, Ph.D. thesis, Massachusetts Institute of Technology (2012).

[8] I. Cziegler, P. H. Diamond, N. Fedorczak, P. Manz, G. R. Tynan, M. Xu, R. M. Churchill, A. E. Hubbard, B. Lipschultz, J. M. Sierchio, J. L. Terry, and C. Theiler, Physics of Plasmas (1994-present) 20, 055904 (2013).

[9] A. White, P. Phillips, D. Whyte, A. Hubbard, C. Sung, J. Hughes, A. Dominguez, J. Terry, and I. Cziegler, Nuclear Fusion 51, 113005 (2011).

[10] J. R. Walk, J. W. Hughes, A. E. Hubbard, J. L. Terry, D. G. Whyte, A. E. White, S. G. Baek, M. L. Reinke, C. Theiler, R. M. Churchill, J. E. Rice, P. B. Snyder, T. Osborne, A Dominguez, and I. Cziegler, Physics of Plasmas 21, 056103 (2014).

[11] X. Q. Xu, B. D. Dudson, P. B. Snyder, M. V. Umansky, and H. Wilson, Phys. Rev. Lett., **105**, 175005 (2010).

[12] X. Q. Xu, B. D. Dudson, P. B. Snyder, M. V. Umansky, H. Wilson and T. Casper, Nucl. Fusion, **51**, 103040 (2011).

[13] Z. X. Liu, X. Q. Xu, X. Gao, T. Y. Xia, I. Joseph, W. H. Meyer, S. C. Liu, G. S. Xu, L. M. Shao, S. Y. Ding, G. Q. Li and J. G. Li, Physics of Plasmas, 21, 090705 (2014);

[14] T.Y. Xia, X.Q. Xu and P.W. Xi, Nucl. Fusion 53, 073009 (2013) .

[15] M.V. Umansky, R.H. Cohen, L.L. LoDestro, X.Q. Xu, Contrib. Plasma Phys. 48, 27 (2008)

[16] B. A. Carreras, L. Garcia, and P. H. Diamond, Phys. Fluids 30, 1388 (1987).

[17] B.D. Dudson, M.V. Umansky, X.Q. Xu, P.B. Snyder, H.R. Wilson, Computer Physics Communications 180, 1467–1480 (2009),

[18] D. P. Fulton, Z. Lin, I. Holod, and Y. Xiao, Physics of Plasmas 21, 042110 (2014).

[19] B. Scott, New Journal of Physics, 4, 52.1-52.30 (2002)

[20] R. H. Kraichnan, Phys. Fluids, 10, 1417 (1967).

[21] Lin, Y., Irby, J., Stek, P., Hutchinson, I., Snipes, J., Nazikian, R., et al. 70, 1078-81 (1999).

[22] Z. X. Liu et al, 57th APS DPP, GO4.00005 (2015).

[23] J. F. MA, The macro- and micro-instabilities in the pedestal region of the Tokamak, Ph.D. thesis, The University of Texas (2015).